High Temperature Steam Corrosion of Cladding for Nuclear Applications: Experimental

ICACC 2013

Kevin M. McHugh
John E. Garnier
Sergey Rashkeev
Michael V. Glazoff
George W. Griffith
Shannon M. Bragg-Sitton

January 2013

The INL is a
U.S. Department of Energy
National Laboratory
operated by
Battelle Energy Alliance

Idaho National
Laboratory

# HIGH TEMPERATURE STEAM CORROSION OF CLADDING FOR NUCLEAR APPLICATIONS: EXPERIMENTAL

Kevin M. McHugh, John E. Garnier, Sergey Rashkeev, Michael V. Glazoff, George W. Griffith, and Shannon M. Bragg-Sitton, Idaho National Laboratory, Idaho Falls, ID, USA

ABSTRACT

Stability of cladding materials under off-normal conditions is an important issue for the safe operation of light water nuclear reactors. Metals, ceramics, and metal/ceramic composites are being investigated as substitutes for traditional zirconium-based cladding. To support down-selection of these advanced materials and designs, a test apparatus was constructed to study the onset and evolution of cladding oxidation, and deformation behavior of cladding materials, under loss-of-coolant accident scenarios. Preliminary oxidation tests were conducted in dry oxygen and in saturated steam/air environments at 1000°C. Tube samples of Zr-702, Zr-702 reinforced with 1 ply of a β-SiC CMC overbraid, and sintered α-SiC were tested. Samples were induction heated by coupling to a molybdenum susceptor inside the tubes. The deformation behavior of He-pressurized tubes of Zr-702 and SiC CMC-reinforced Zr-702, heated to rupture, was also examined.

INTRODUCTION

A primary requirement of advanced nuclear fuel cladding designs is to contain the nuclear fuel inside the fuel rods in the event of a loss-of-coolant accident (LOCA) without diminishing heat transfer characteristics or impairing coolant flow during normal operation. This critical function would increase the safety margin of nuclear reactor designs significantly. While Zr-based alloys are currently used as cladding in most nuclear reactor designs, a variety of advanced cladding materials including metals, ceramics and metal/ceramic composites are being considered as replacements. The corrosion behavior of these materials depends on many factors, including the chemical nature of the cladding material, the reaction temperature, and the type and concentration of the oxidizing agent. For example, corrosion of Zr in air follows a different oxidation pathway than it does in steam. In air, the predominant reaction is:

$$Zr\ (s) + O_2(g) \rightarrow ZrO_2\ (s).$$
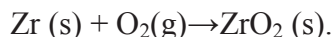
In steam, oxidation is accompanied by the evolution of hydrogen gas which can potentially ignite:

$$Zr(s) + 2H_2O(g) \rightarrow ZrO_2\ (s) + 4H_2\ (g)$$
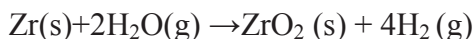
During a LOCA, zirconium fuel cladding can rapidly heat up to temperatures exceeding 1000°C due to redistribution of fuel thermal energy and fission product decay heating. Steam/cladding interactions above the α/β transformation temperature (~815°C) result in increased oxygen transport inside the metal, the formation of the brittle oxygen-stabilized α phase, and growth of a brittle ZrO$_2$ film on the outside of the cladding. The metal can swell and rupture or fracture during refill quenching, exposing the reactor's primary coolant loop to the fuel.

A number of techniques have been developed over the years to evaluate the oxidation behavior of Zr-based cladding materials in steam and air/oxygen. Early ductility studies by

Hobson and Rittenhouse[1], and metallographic analysis by Pawel[2], led to the adoption of the 17% oxidation criterion, the 1204°C criterion, and Baker-Just oxidation rate correlation.[3,4] These studies examined oxygen uptake above the (α + β)/ β transformation temperature and the formation of the brittle oxygen stabilized α phase.

Silicon carbide exhibits excellent radiation stability, is composed of low activation elements, and retains its strength and shape under high radiation dose conditions. It is used in advanced nuclear fuel element designs to provide high thermal conductivity containment and structural support to oxide-based fuel. Tristructural Isotropic (TRISO) coated fuel particles used in gas-cooled reactors contain one layer of SiC and three layers of pyrolytic carbon surrounding the fuel kernel. Here the SiC acts as a pressure vessel for fission products, providing structural integrity while retaining solid fission products inside the fuel pellet.[5] All-SiC fuel rod cladding designs are in the development and testing stage for use in light water reactors.[6] Zr-based fuel rods over-braided with SiC ceramic matrix composites could also provide additional structural support, increasing the margin of safety of the metal fuel rods (Figure 1).[7]

SiC is more stable than Zr in air and steam environments, and provides the potential for greater structural stability in a LOCA. Researchers have studied the corrosion behavior of high purity CVD SiC in steam and oxygen and have found that corrosion behavior differs substantially.[8] Corrosion in dry oxygen involves the formation of a relatively stable SiO_2 layer:

$$2SiC(s) + 3O_2(g) \rightarrow 2SiO_2 + 2CO(g)$$
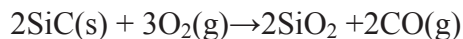
Further oxidation is limited by the oxygen diffusion rate through silica. This layer thus protects the underlying SiC, as the diffusion rate is low. In contrast, the introduction of water vapor allows hydrolysis of SiO_2 to occur, and corrosion of SiC proceeds more rapidly following a two-step oxidation/volatilization reaction[9]:

$$SiC (s) + 3H_2O(g) = SiO_2(s) + 3H_2(g) + CO(g) \qquad (1)$$

$$SiO_2 (s) + 2 H_2O (g) = Si(OH)_4 (g) \qquad (2)$$
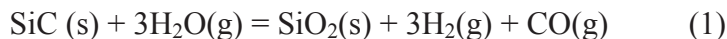
Since the $Si(OH)_4$ is volatile, the recession rate of SiC is greater. The kinetics of the oxidation reaction are described by a parabolic rate constant, while the kinetics of volatilization are described by a linear rate constant. As the partial pressure of water vapor increases, the corrosion rate increases.[10] The SiC recession rate accelerates with rising temperature.

The potential benefits of advanced ceramic and composite materials in the design of nuclear reactor components underscores the need to contrast corrosion behavior of these materials with conventional zirconium-based materials in LOCA scenarios under identical test conditions.
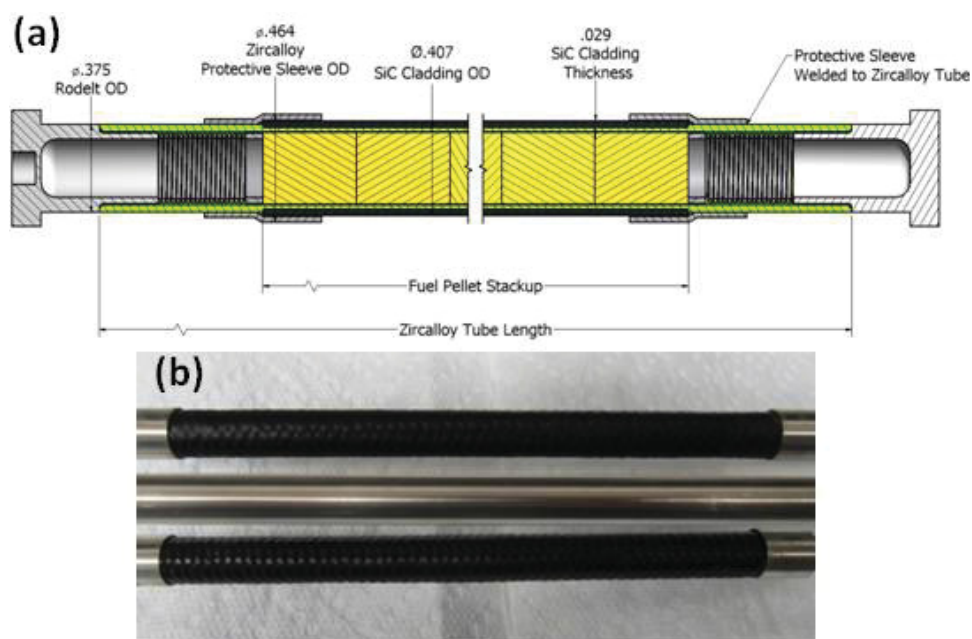
Figure 1. (a) Cladding assembly design, and, (b) fabricated samples of Zircaloy-4 overbraided with 1-ply and 2-ply SiC/SiC ceramic matrix composites (CMCs).[11]

EXPERIMENTAL

The test apparatus used in this study, referred to as the Oxidation Kinetics System (OKS), has been described previously.[12] The system tracks and catalogs outputs from various pressure, temperature and gas composition sensors while exposing heated fuel cladding samples to water/steam, water/air or other oxidation environments. One-color and two-color pyrometers, in conjunction with a thermal image system and thermocouple signals, track the onset of oxidation via emissivity changes at the surface of the cladding. These instruments also sense the exothermic/endothermic reactions that accompany oxidation and phase changes. Gas-phase reaction products of oxidation (e.g., H_2 and CO) are monitored and correlated with temperature/emissivity changes. In addition, nonvolatile or water-soluble oxidation products are collected in a condenser and evaluated off-line.

Te following samples were oxidized in air that was saturated with steam inside a sealed chamber:

1. Closed Zr-702 tubes, pressurized with He to 3.4 MPa and heated at a rate of 37^OC/min to bursting.
2. Closed Zr-702 tubes with 1" sleeves of 1ply SiC/SiC CMC. These composite tubes were pressurized with He to 3.4 MPa and heated to bursting at a rate of 37^OC/min.
3. Open tubes of Zr-702 heated to 1000^OC at a rate of 37^OC/min and held for one hour.

Additional samples were tested in dry oxygen. These samples were heated at a rate of about 5^OC/min in argon to 1000^OC and exposed to dry oxygen for 10 minutes:

1. Open tubes of sintered α-SiC.
2. Open tubes of Zr-702.

The Zr-702 tubes were vertically oriented and fixed at one end. The other end was attached to a pressurized helium gas source via a flexible stainless steel 316L gas line. Helium used to

pressurize the samples was ultra high purity. High purity dry oxygen was used in the dry oxygen experiments. High purity (nanopure) water having chemistry characteristics similar to the primary coolant loop of INL's Advanced Test Reactor (ATR) was used to generate steam inside the closed system. The water's pH = 5.1, dissolved oxygen = 5.5 ppm, and conductivity = 3.2 μS/cm were measured using temperature compensated probes for pH (Rosemont Analytical 3500VP sensor), dissolved oxygen (Rosemont Analytical HX438 sensor) and conductivity (Rosemont Analytical 400 sensor).

The CMCs were fabricated by polymer infiltration and pyrolysis (PIP) of a 1-ply woven fabric of Hi Nicalon using polycarbosilane.[13] Both the fibers and the matrix were β-SiC. Commercial pressureless-sintered α-SiC tube samples were formed from ~6 μm power to 98% density using boron and carbon sintering aids.[14] Figure 2 compares the surface appearance of the SiC samples used in this study.

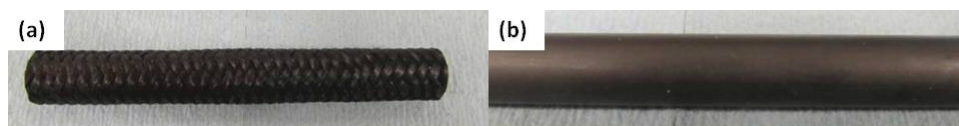Figure 2. SiC tube samples used in this study. (a) CMC sleeve formed from woven β-SiC fibers that was used to reinforce Zr-702 tubes during deformation testing. (b) α-SiC tube.

Commercial Zr-702 tubes (Zircadyne™ 702, UNS Designation R60702) measuring 9.5 mm OD x 7.6 mm ID x 356 mm were used.[15] The alloy contains up to 4.5 wt.% Hf in solid solution, with the following maximum limits of other elements: Fe+Cr (0.20%), H (0.005%), N (0.025%), C (0.05%), and O (0.16%). While the Hf content of the alloy precludes its use in a nuclear reactor, it was chosen due to cost and availability for these preliminary studies.

Samples were induction heated from the inside-out by coupling to a 7.5 mm OD x 254 mm long molybdenum rod placed inside the tubes. The gap between the Mo and cladding was chosen to be similar to the gap between fuel pellets and cladding in a typical pressurized water reactor (PWR). Temperature was measured using type K thermocouples placed 25 mm inside the Mo susceptor, as well as at the center of the Zr tube and 50 mm above the center of the tube.

RESULTS AND DISCUSSION

Oxidation in steam/air and dry oxygen at 1000°C.
Figure 3 illustrates the surface oxidation of Zr-702 tubing after one hour exposure to steam/air at 1000°C.

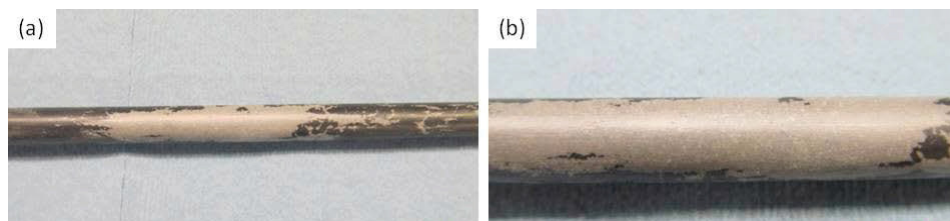Figure 3. Surface oxidation of Zr-702 tubing following one hour exposure to steam/air at ~1000°C.

The mottled surface was characterized by a white, flaky, fully-converted ZrO_2 product and a tenacious black transitional zirconium oxide layer. Tube samples were sectioned along the length at 25 mm increments from the center of the tube to the edge of the induction heated zone (254 mm). Similar

microstructure features were observed for all samples. Figure 4 shows representative SEM photomicrographs of the cross-section of tubing, at various magnifications. Three main microstructure zones were observed as oxygen diffuses into the alloy at 1000^OC: an outer, fully-converted zirconium oxide layer; a partially converted underlying zone of oxygen-stabilized α-Zr phase; and a minimally oxidized β-Zr phase of the base metal. The fully converted zirconium oxide layer was about 65 μm thick and was interlaced with axial and transverse cracks of various lengths that resulted from tensile loading due to volumetric expansion. Use of a vCD detector (BSE mode) in Figure 4d clearly revealed these cracks as well as transverse cracks which initiated in the brittle, oxygen-stabilized, α-Zr phase of the metal. The oxygen-stabilized, α-Zr phase was less well resolved but appeared to be about 30 μm thick. Similar trends have been observed by other investigators in steam-oxidized Zircaloy-2 [4, 18] and Zircaloy-4.[16,17, 19] The relative thickness of the fully converted oxide layer and O-stabilized α phase will depend on temperature and time. Weight gain measurements in these studies indicated that the total oxygen uptake for samples tested at 1000^OC obeys a parabolic rate law, $W^2 = K_p t$ where K_p is the temperature dependent rate constant, W denotes oxygen weight gain, and t is time. The current study was conducted in acidified steam (simulating a LOCA at INL's ATR reactor). It is not clear to what extent this affected the oxidation behavior.
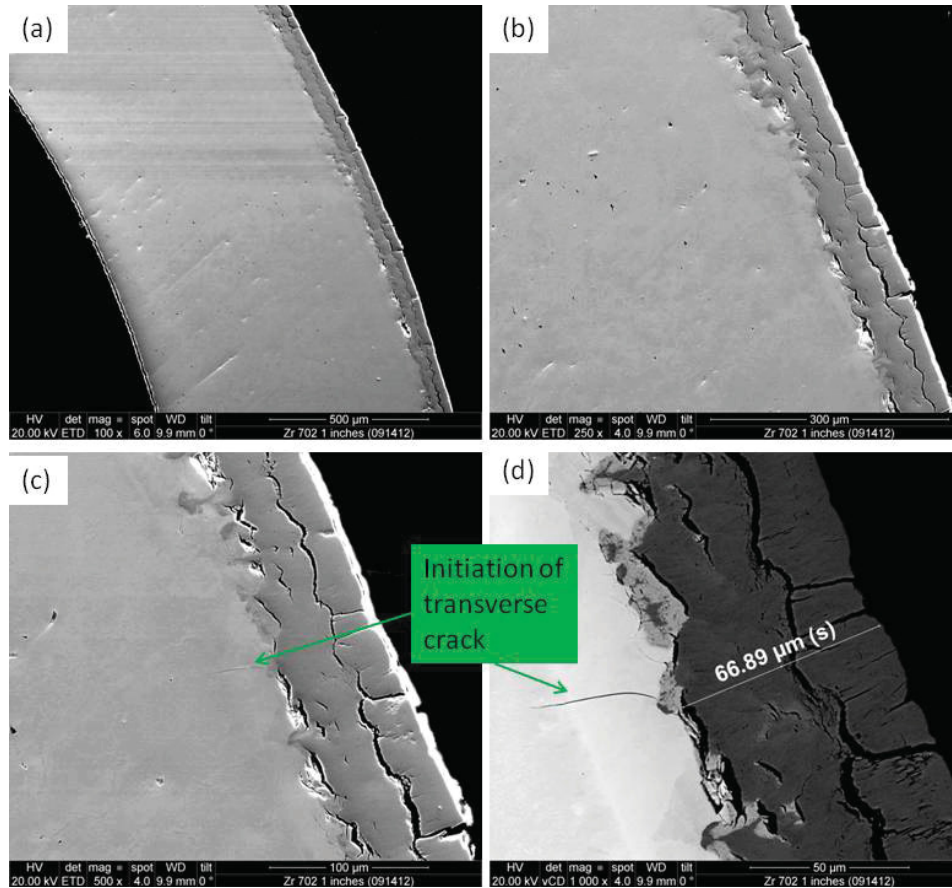

Figure 4. SEM photomicrographs of Zr-702 tubing following one hour exposure in air/supersaturated steam at ~1000^OC. (a) 100X, secondary electron mode. (b) 250X, secondary electron mode. (c) 500X, secondary electron mode. (d) 1000X, backscattered electron mode.

EDS element mapping analysis was performed on a cross-section of oxidized tubing to determine the transition in composition from the outer edge of the tube to the interior. Nine scans, each 2.5 min/scan, and evenly spaced by 14.6 μm, were taken progressing from the center of the oxide layer to about 117 μm into the interior of the sample. Figure 5 summarizes concentration data of O, Zr, Cr, Fe, and Hf.

Spot #	O (wt%)	Zr (wt%)	Cr (wt%)	Fe (wt%)	Hf (wt%)
1	0.83	92.3	0.32	0.34	2.13
2	0.79	92.1	0.37	0.43	2.12
3	1.14	92.08	0.32	0.38	2.00
4	1.33	91.78	0.32	0.42	1.79
5	1.87	91.11	0.35	0.40	2.08
6	2.60	90.75	0.30	0.37	1.88
7	3.17	90.16	0.30	0.36	1.86
8	14.37	79.71	0.21	0.27	1.43
9	14.98	79.79	0.03	0.12	1.17

Figure 5. EDS element probe data taken on a Zr-702 sample following one hour exposure to air/supersaturated steam at ~1000°C. (a) SEM photomicrograph showing sampling locations. (b) Wt.% data for O, Zr, Cr, Fe and Hf at various sampling locations.

There is a steep drop in the oxygen concentration from the largely converted ZrO_2 to the O-stabilized α-Zr. This is followed by a gradual decrease in the prior β-Zr region of the interior. The concentrations of Cr, Fe, and Hf in these regions follow a similar pattern. As the layer of O-stabilized α-Zr grows, β-stabilizing elements such as Cr and Fe preferentially diffuse into the β-Zr phase at a high diffusion rate.

Additional samples of Zr-702 and sintered α-SiC were heated to 1000°C in argon and then exposed to high purity, dry oxygen for 10 minutes. Figure 6 compares the microstructures near the edge of a Zr-702 tube (Figure 6a) and pressureless sintered α-SiC (Figure 6b). The Zr-702 sample formed a brittle ZrO_2 layer at the exposed surface measuring about 40 μm thick. Both axial and transverse cracks are present, along with evidence of spalling and delamination. The adjacent oxygen-stabilized α-Zr phase is also about 40 μm thick and appears to be uniform in thickness. Transverse cracks are seen in this layer. Optical microscopy also reveals significant coarsening of the β-Zr phase in the interior of the sample due to the slow heating rate. The α-SiC sample (Figure 6b) has formed a relatively thin layer of SiO_2 that appears to be of variable thickness.
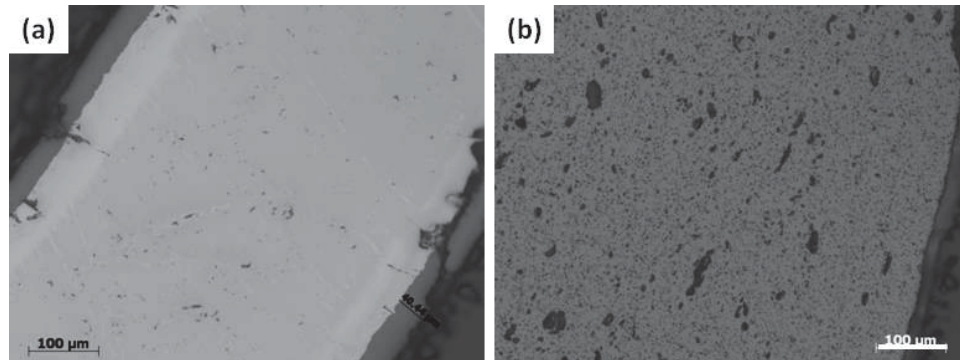

Figure 6. Optical photomicrographs of (a) Zr-702, and, (b) pressureless sintered α-SiC following a 10 minute exposure to dry oxygen at 1000°C.

Figure 7 compares the microstructure of etched Zr-702 samples viewed with polarized light. The starting material, shown in Figure 7a, is characterized by a uniform, relatively fine-grained α-Zr phase, with small, uniformly distributed second- phase particles. During oxidation at 1000°C in steam (Figure 7b) or oxygen (Figure 7c), a relatively coarse O-stabilized α-Zr phase formed. A sharp interface forms with the β-Zr because β phase stabilizers such as Fe and Cr diffuse into the β-Zr, as shown in Figures 7 b and 7c. The slow heating rate for the sample oxidized in dry oxygen caused the β-Zr phase to coarsen.
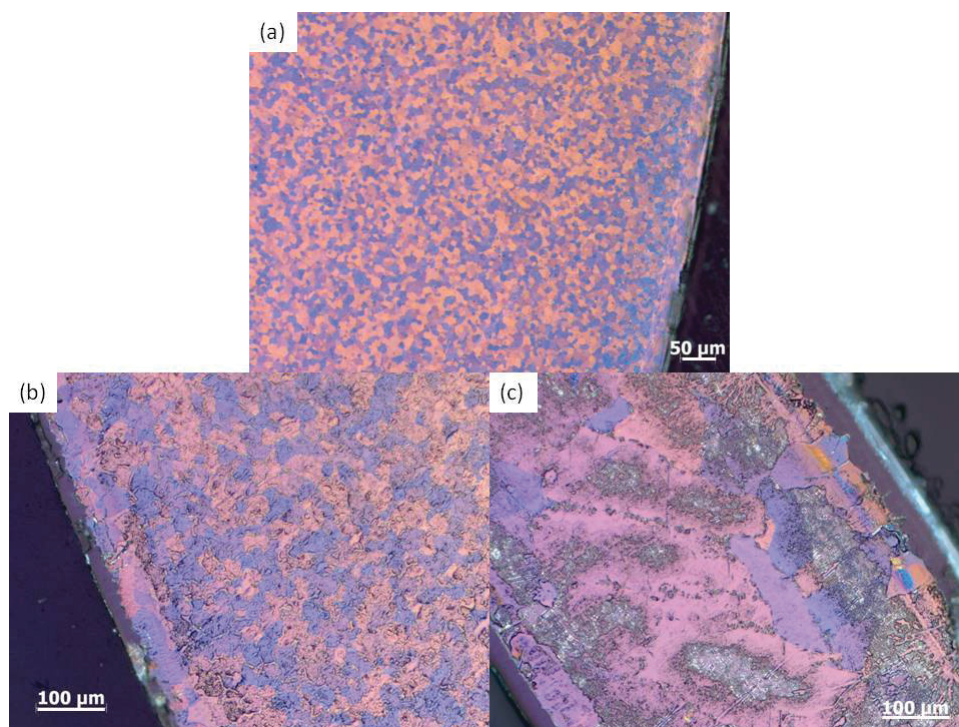
Figure **7**. Optical photomicrographs of etched Zr-702 tubing cross sections viewed with polarized light. (a) As-received commercial tubing. (b) Oxidized in steam/air. (c) Oxidized in dry oxygen.

Deformation of pressurized tubes

Nuclear fuel rods used in a PWR are internally pressurized with He to about 2 MPa during manufacture. Helium is added to improve thermal conductivity at the pellet-cladding interface, and to reduce interaction between pellet and cladding during service. As the tubes are heated, the pressure rises. As the fuel ages, gaseous fission products further increase the pressure. The internal pressure is largely offset by the water pressure in the reactor's primary coolant loop. During a LOCA, as primary coolant is lost, the rise in differential pressure can cause the cladding to strain and rupture. Advanced materials such as SiC CMC could increase the reactor's safety margin by providing containment for the nuclear fuel, preventing it from entering the primary coolant.

Deformation of fuel cladding during a LOCA is very complicated. Stress, temperature, and creep strength influence deformation. Azimuthal (circumferential) temperature variations due to fuel movement and eccentricity can play an important role in local temperature and strain behavior. Manufacturing flaws and small differences in microstructure also influence creep. Various studies have been conducted worldwide to study the deformation and ballooning behavior of zirconium alloys in steam, for example, at the PROPAT facility in the UK[20], the EDGAR-1[21] and EDGAR-2[22] facilities in Canada and at CEA in France, the Korean Atomic Energy Institute[23], Japan[24], and elsewhere.

Preliminary experiments were conducted in steam/air on pressurized tubes of Zr-702 measuring 9.5 mm OD x 356 mm long. As-received Zr-702 tubes and Zr-702 tubes reinforced with a ~ 38 mm long tubular sleeve of SiC CMC, as shown in Figure 2a, were tested. The composite tube consisted of single-ply Hi Nicalon β-SiC woven fibers that were polymer-infiltrated with polycarbosilane and pyrolyzed to form a matrix of β-SiC. Tubes were pressurized

7

with He to 3.4 MPa and induction heated to the point of rupture by coupling the induction field to a 254 mm long Mo rod susceptor inserted inside the Zr-702 tubes at the center. Temperature of the susceptor was monitored with a grounded type K thermocouple inserted 25 mm from the end of the susceptor. Tubes were heated at an average rate of 37^OC/min.

Figure 8a shows an as-received (starting) Zr-702 tube, and ruptured sample, while Figure 8b shows a starting Zr-702 tube with a 11 mm ID x 11.3 mm OD x 38 mm long SiC CMC sleeve. The sleeve fit loosely over the Zr-702 tube with about 1.5 mm clearance. Since the tubes were vertically oriented, a small ring of a ZrO_2–based adhesive was applied to the Zr-702 tube to center the SiC CMC sleeve and hold it in place. The coating ring appears white in Figure 8b, to the left of the SiC CMC.

Figure 8. Photographs of starting samples (above) and ruptured samples (below) of (a) Zr-702 tube, and, (b) Zr-702 tube fitted with a SiC CMC sleeve.

Rupture of the unreinforced tube occurred at about 850^OC, 13 mm from the center of the tube, and was accompanied by a loud popping sound of tearing metal and rapid pressure drop (Figure 9a). A second unreinforced tube ruptured at 896^OC, 93 mm from the center of the tube (Figure 8a). The metal samples ballooned and ruptured in a similar way, with axial tears measuring about 17 mm and 10 mm, respectively. Swelling was observed along the entire length of the tube. Zr-702 in the HCP structure (α phase) transforms to the BCC structure (β phase) at 865^OC. The presence of β phase reduces the strength substantially. Similar results have been observed with rupture tests conducted on Zircaloy cladding metal tubes, i.e., rupture occurs as the metal transitions into the α + β phase field.

Identical experimental conditions were used to evaluate two samples reinforced with 1-ply SiC CMC sleeves. The samples ruptured at somewhat higher temperatures, about 920^OC and 914^OC. The ruptured area of the reinforced samples was small and pin-hole shaped, and was accompanied by a somewhat slower, inaudible release of pressure. The ruptures occurred 5 mm and 7 mm from the center of the tubes, respectively. Notable swelling occurred along the length of the Zr-702 tube except where the tube was reinforced with the SiC CMC sleeve.

8

Dimensional data for two deformed tubes, one with and one without a reinforcing SiC CMC sleeve, are given in Figures 9 and 10. Diameters were measured in line with the location of the rupture (Figure 9) and at a 90° rotation (Figure 10) for the same samples. Swelling occurred along the entire length of the tubes where they were internally heated. The samples ballooned at the location of the rupture with a maximum circumferential strain of about 80%. This is significant considering that the spacing of fuel rods in a typical PWR design is such that adjacent rods strained by about 32% will touch. At the location of the reinforcing SiC CMC sleeve, metal expansion was significantly constrained. The OD increased about 2%, indicating the 1-ply braided SiC CMC fabric stretched slightly but did not fail under the test conditions.

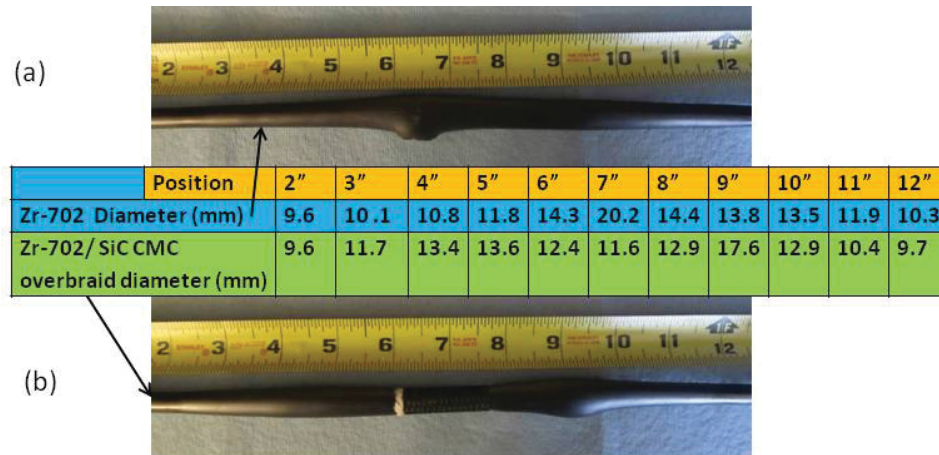| Position	2"	3"	4"	5"	6"	7"	8"	9"	10"	11"	12"
Zr-702 Diameter (mm)	9.6	10.1	10.8	11.8	14.3	20.2	14.4	13.8	13.5	11.9	10.3
Zr-702/ SiC CMC overbraid diameter (mm)	9.6	11.7	13.4	13.6	12.4	11.6	12.9	17.6	12.9	10.4	9.7

Figure 9. Dimensional data for ruptured Zr-702 tubes. Diameter measurements were made in-line with the location of the rupture. (a) Unreinforced Zr-702 tube. (b) Zr-702 tube reinforced with a 38 mm long x 11.3 mm OD SiC CMC sleeve at the center.

Figure 10. Dimensional data for ruptured Zr-702 tubes. Diameter measurements were made at 90° rotation to the location of the rupture. (a) Unreinforced Zr-702 tube. (b) Zr-702 tube reinforced with a 38 mm long x 11.3 mm OD SiC CMC sleeve at the center. Expanded views at the rupture locations are shown.
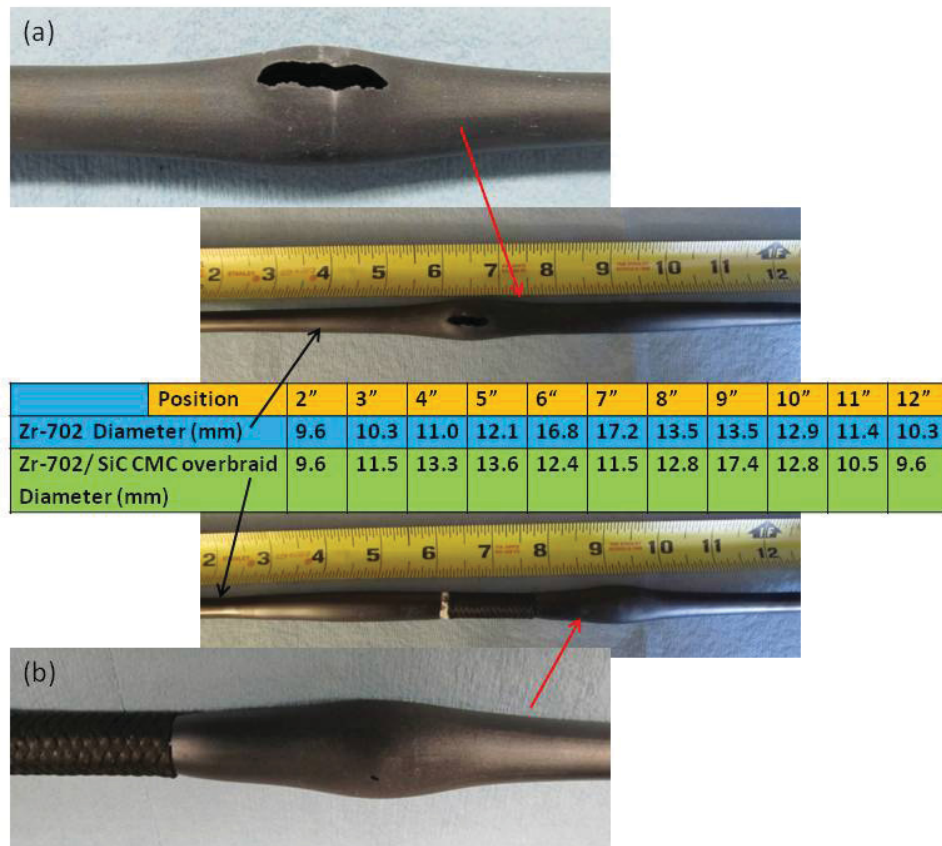
CONCLUSIONS

A newly designed test apparatus referred to as the Oxidation Kinetics System (OKS) was used in this study. The system exposes nuclear fuel cladding materials to out-of-reactor, simulated LOCA conditions to study the onset and evolution of oxidation, deformation behavior and quenching behavior.

Preliminary tests were conducted using Zr-702 and SiC ceramic materials. The SiC materials were sintered α-SiC and a β-SiC / β-SiC CMC composed of Hi Nicalon fibers in a matrix of pyrolyzed polycarbosilane. As expected, SiC exhibited improved oxidation resistance over Zr-702 in dry oxygen and steam/air at 1000^OC. Oxygen and steam readily attacked Zr-702 forming a brittle ZrO_2 layer at the exposed surface interlaced with axial and transverse cracks. Oxygen diffusion through this layer resulted in the formation of an oxygen-stabilized α-Zr phase with intermittent transverse cracks. The interior of the Zr-702 transformed to the β-Zr phase which coarsened with exposure time at elevated temperature. The SiC materials formed a thin layer of relatively stable SiO_2.

Preliminary experiments were also conducted in steam/air on pressurized (3.4 MPa He) tubes of Zr-702 and Zr-702 tubes reinforced with a tubular sleeve of SiC CMC. The tubes were induction heated to the point of rupture by coupling the induction field to a Mo susceptor inserted inside the Zr-702 tubes. Rupture occurred as the Zr-702 transitioned into the α + β phase

field. Ballooning was observed for all samples with a maximum circumferential strain of about 80%. At the location of the reinforcing SiC CMC sleeve, metal expansion was significantly constrained. The OD increased about 2%, indicating the 1-ply braided SiC CMC fabric stretched but did not fail under the test conditions.

ACKNOWLEDGEMENT

REFERENCES

[1] D. O. Hobson and P. L. Rittenhouse, "Embrittlement of Zircaloy-Clad Fuel Rods by Steam During LOCA Transients," Oak Ridge National Laboratory, ORNL-4758, January, 1972.

[2] R. E. Pawel, "Oxygen Diffusion in β Zircaloy During Steam Oxidation," *J. Nucl.Mater*. 50 (1974) 247-258.

[3] L. Baker, Jr. and L.C. Just, "Studies of Metal-Water Reactions at High Temperatures. III. Experimental and Theoretical Studies of the Zirconium-Water Reaction," Argonne National Laboratory, ANL 6548, May 1962.

[4] A. F. Brown and T. Healey, "The Kinetics of Total Oxygen Uptake in Steam-Oxidized Zircaloy-2 in the Range 1273-1673 K," *J. Nucl.Mater*. 88 (1980) 1-6.

[5] Lance L. Snead, Takashi Nozawa, Yutai Katoh, Thak-Sang Byun, Sosuke Kondo, and David A. Petti, "Handbook of SiC properties for fuel performance modeling," *J. Nucl. Mater*. 371 (2007) 329-377.

[6] Herbert Feinroth and Bernard R. Hao, "Multi-layered ceramic tube for fuel containment barrier and other applications in nuclear and fossil power plants," Westinghouse Electric, July 2006: WO 2006/076039.

[7] John E. Garnier and George W. Griffith, "Cladding Material, Tube Including Such Cladding Material and Methods of Forming the Same," U. S. Patent Application Attorney Docket 2939-10060US (BA-477).

[8] Nathan Jacobson, Dwight Myers, Elizabeth Opila and Evan Copland, "Interactions of Water Vapor with Oxides at Elevated Temperatures," *J. Phys. Chem. Solids* 66 (2005) 471-478.

[9] Elizabeth J. Opila, "Oxidation and Volatilization of Silica Formers in Water Vapor," *J. Am. Ceram. Soc., 86* (2003), 1238-48.

[10] Elizabeth J. Opila, "Variation of the Oxidation Rate of Silicon Carbide with Water-Vapor Pressure," *J. Am. Ceram. Soc., 82* (1999), 625-36.

[11] INL/MIS-12-25696 LWRS Fuel Development Plan.

[12] INL/EXT -12-27209.

[13] Physical Sciences, Inc., Andover, MA, USA.

[14] Saint-Gobain Ceramics, Niagara Falls, NY, USA.

[15] Allegheny Technologies, Inc., Pittsburgh, PA, USA.

[16] J. H. Baek, K. B. Park and Y. H. Jeon, "Oxidation kinetics of Zircaloy-4 and Zr-1 Nb-1Sn-0.1Fe at temperatures of 700-1200°C," *J. Nucl.Mater*. 335 (2004) 443-456.

[17] J. H. Baek and Y. H. Jeon, "Steam oxidation kinetics of Zr-1.5 Nb-0.4Sn-0.2Fe-0.1Cr and Zircaloy-4 at 900-1200°C," *J. Nucl.Mater*. 361 (2007) 30-40.

[18] K. Pettersson and Y. Haag, "Deformation and Failure of Zircaloy Cladding in a LOCA. Effects of Preoxidation and Fission Products on Deformation and Fracture Behavior. SKI project B23/78," Studsvik Energiteknik AB, STUDSVIK/K4-80/13, March 1980.

[19] R. R. Biederman, et. al., "A Study of Zircaloy-4 – Steam Oxidation Kinetics," EPRI NP-734 Final Report, April, 1978.

[20]E. D. Hindle and C. A. Mann, "An Experimental Study of the Deformation of Zircaloy PWR Fuel Rod Cladding Under Mainly Convective Cooling," Zirconium in the Nuclear Industry: Fifth Conference, 1980, Boston, MA, USA, ASTM STP 754, ASTM, pp. 284-302.

[21] S. Sagat, H. E. Sills, and J. A. Walsworth, "Deformation and Failure of Zircaloy Fuel Sheaths Under LOCA Conditions," Zirconium in the Nuclear Industry: Sixth International Symposium, 1982, Vancouver, Canada, ASTM STP 824, ASTM pp. 709-733.

[22] T. Forgeron et. al., "Experiment and Modeling of Advanced Fuel Rod Cladding Behavior Under LOCA Conditions: A-B Phase Transformation Kinetics and EDGAR Methodology," Zirconium in the Nuclear Industry: Twelfth International Symposium, 1998, Toronto, Canada, ASTM STP 1354, ASTM pp. 256-278.

[23]J. H. Kim, et. al., "Embrittlement Behavior of Zircaloy-4 Cladding during Oxidation and Water Quench," Nuclear Engineering and Design, 235 (2005) 67-75.

[24]T. Furuta et. al., "Zircaloy Clad Fuel Rod Burst Test Behavior under Simulated Loss of Coolant Conditions in PWRs," *J. Nucl. Sci. Technol.*, 15, (1978), 736-744.